Faraday Discussions

Accepted Manuscript

This manuscript will be presented and discussed at a forthcoming Faraday Discussion meeting. All delegates can contribute to the discussion which will be included in the final volume.

Register now to attend! Full details of all upcoming meetings: http://rsc.li/fd-upcoming-meetings

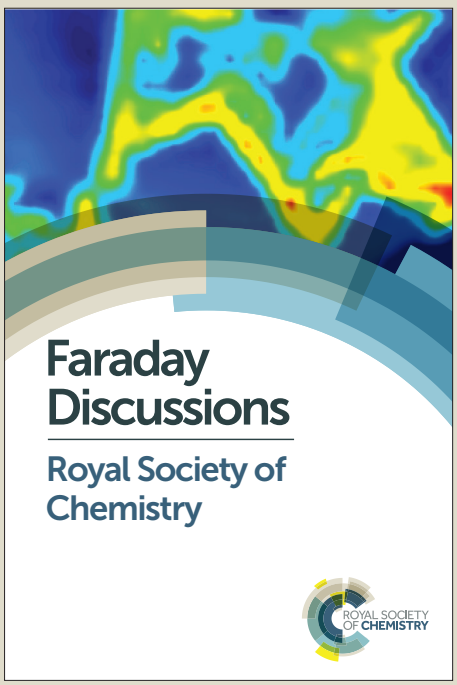

This is an *Accepted Manuscript*, which has been through the Royal Society of Chemistry peer review process and has been accepted for publication.

Accepted Manuscripts are published online shortly after acceptance, before technical editing, formatting and proof reading. Using this free service, authors can make their results available to the community, in citable form, before we publish the edited article. We will replace this *Accepted Manuscript* with the edited and formatted *Advance Article* as soon as it is available.

You can find more information about *Accepted Manuscripts* in the Information for Authors.

Please note that technical editing may introduce minor changes to the text and/or graphics, which may alter content. The journal's standard Terms & Conditions and the Ethical guidelines still apply. In no event shall the Royal Society of Chemistry be held responsible for any errors or omissions in this *Accepted Manuscript* or any consequences arising from the use of any information it contains.

ROYAL SOCIETY OF CHEMISTRY

www.rsc.org/faraday_d

Journal Name

RSCPublishing

ARTICLE

Controlling factors in localised corrosion morphologies observed for magnesium immersed in chloride containing electrolyte

Cite this: DOI: 10.1039/xoxxoooooox

Received ooth January 2012,
Accepted ooth January 2012

DOI: 10.1039/xoxxoooooox

www.rsc.org/

Geraint Williams*[a], Nick Birbilis[b] and H. Neil. McMurray[a]

The early stages of localised corrosion affecting magnesium (Mg) surfaces when immersed in aqueous sodium chloride (NaCl) solutions involves the propagation of dark regions, within which both anodic metal dissolution and cathodic hydrogen evolution occur. For nominally "pure" Mg, these dark areas can either take the form of discs which expand radially with time, or filiform-like tracks which lengthen with time. For Mg surfaces which display disc-form corrosion features in concentrated NaCl electrolyte, a transition to filiform corrosion (FFC) is observed as the concentration is decreased, indicating ohmic constraints on radial propagation. A similar effect is observed when Mg specimens of different iron impurity are immersed in a fixed, high concentration NaCl solution, where disc-form corrosion is observed on samples having ≥ 280 ppm Fe, but FFC predominates at ≤ 80 ppm Fe. An in-situ scanning vibrating electrode technique (SVET) is used to determine current density distributions within the propagating corrosion features. Cathodic current density values of between -100 and -150 Am^{-2} measured in central areas of disc-like features are sufficient to sustain the radial growth of a local anode at the perimeter of the discs. However, for high purity Mg specimens (≤ 80 ppm Fe), cathodic current densities of -10 A m^{-2} or less are measured over FFC affected regions, indicating that linear propagation arises when there is insufficient cathodic current produced on the corroded surface to sustain radial growth. The results are consistent with surface control of localised corrosion propagation in high throwing power electrolyte, but ohmic control in dilute, lower conductivity NaCl solution.

Introduction

Localised corrosion affecting magnesium (Mg) and its alloys is particularly visually striking since it involves the evolution of black areas which grow with time and eventually consume the entirety of the original lustrous surface [1-5]. Although numerous publications are devoted to the subject of Mg corrosion, comprehensively reviewed elsewhere [6-13], studies of surface morphology changes during corrosion have received relatively little attention compared with electrochemical and microscopic investigations. Nevertheless, recently published works have highlighted the significance of the propagating dark areas and the importance of the role that this transformation plays in determining corrosion rate [2-4]. It is currently accepted that the dark corroded regions, which develop following breakdown of a partially-protective hydr(oxide) film formed upon initial immersion, show considerably enhanced electro-catalytic activity towards cathodic hydrogen evolution when compared with the uncorroded surface [2-5,14]. As a consequence, instantaneous Mg corrosion rates rise with immersion time as a progressively greater area of the original intact exposed surface becomes converted to the darkened, corroded form. Recent studies have shown that this effect is particularly evident under circumstances where the Mg surface is anodically polarised [4,5 14-17]. Progressively higher rates of hydrogen evolution, observed with increasingly positive potentials or higher applied anodic currents, are explained on the basis of a more rapid conversion of the uncorroded Mg to a dark cathodically enhanced surface [4]. In turn, higher growth rates of cathode areas and an associated increase total cathodic current preclude the need to explain the electrochemical behaviour of dissolving Mg surfaces in terms of a contentious mechanism involving an Mg^{+} intermediate [18-23].

In publications where observations on the evolution of Mg or Mg alloy corrosion morphologies are discussed, there appear to be considerable variations in the type of dark features which characterise localised corrosion propagation. Observations of dark, thread-like tracks, which evolve hydrogen and lengthen

Faraday Discussions Accepted Manuscript

with time, are described for pure Mg samples immersed in dilute chloride-containing aqueous solutions [24,25]. For a selection of magnesium alloys, including Mg-Al-Zn [26,27], Mg-Zn-Y [28], Mg-Li [29] and AZ31B [30], filiform corrosion (FFC) is reported under conditions of significantly higher chloride ion concentration. However, other investigations involving both pure Mg [2,5,20] and Mg-Nd alloys [31] describe the evolution of dark disc-like areas which expand with time and evolve hydrogen from within their interiors. In this work we seek to elucidate the underlying reasons which dictate localised corrosion behaviour for unpolarised Mg specimens using 2 different types of approach. In the first a commercially available Mg sample type, which displays disc-form evolution of localised corrosion in concentrated aqueous sodium chloride solution, is subjected to a combination of in-situ scanning vibrating electrode and close-up time-lapse photography to investigate the influence of electrolyte concentration on localised corrosion morphology. Changes in time-dependent current density distributions associated with the transition from disc-like to filiform corrosion, observed with decreasing sodium chloride concentration, are used to explain the observed transformation in morphology. In the second approach, the same combination of techniques is used in a fixed, high concentration NaCl (aq) electrolyte to explain the change from disc-form to FFC morphology observed for Mg specimens containing varying iron impurity composition. The magnitude of local cathodic currently density measured over dark-corroded regions is used to develop theories which demonstrate ohmically limited propagation in dilute NaCl electrolyte and cathodically controlled propagation in concentrated solution.

Experimental Details

Materials. Commercial purity (CP) magnesium foil (99.9+%, 25 mm square coupons of 1 mm thickness) was obtained from Goodfellow Metals Ltd, with the main impurities being iron (280 ppm) and manganese (170 ppm). Alternative higher purity Mg specimens were sourced elsewhere. High purity Mg in the form of a section of 10 mm diameter rod, containing a 40 ppm iron impurity level, was supplied by AMAC (Melbourne, Aus)., while a Mg specimen comprising 80 ppm Fe was provided as a gift by Prof A. Atrens (University of Queensland). A Mg-Fe alloy of roughly 1% w/w composition was prepared by melting commercially pure Mg with fine Fe powder in a crucible at 700°C held in a resistance furnace using AM-Cover® (0.2 wt.% tetrafluoroethane and 99.8 wt.% nitrogen) as a cover gas [32]. The mixture was held in the molten state for several days with intermittent vigorous stirring. Finally, the mixture was homogenised just below the melting point for 3 days. An exact composition of 1.34% w/w for the Mg-Fe alloy was determined independently via ICP-AES (by Spectrometer Services, Coburg, Aus.).

Methods. Scanning vibrating electrode measurements were carried out using a probe comprising a 125 µm diameter platinum wire sealed in a glass sheath so that the active portion of the probe tip consisted of a 125 µm diameter Pt micro-disc electrode and the total tip diameter was ~ 250 µm. The probe vibration frequency was 140 Hz and the peak-to-peak vibration amplitude was 30 ± 5 µm. Full details of the SVET instrument design, mode of operation and calibration are given elsewhere [2,33]. In this work, the SVET peak-to-peak voltage signal was converted to values of current flux density along the axis of probe vibration (j_z), after galvanostatically checking the calibration using a two-compartment cell containing the relevant NaCl (aq) electrolyte, again as described previously [2].

For SVET analysis, the various Mg specimens under investigation were cut into conveniently sized coupons, subjected to grinding using silicon carbide paper and polished using an aqueous slurry of 5 µm polishing alumina. Finally the polished surfaces were washed with aqueous detergent and rinsed with distilled water followed by ethanol. Test samples were then prepared by covering the surface with 90 µm thick extruded PTFE 5490 tape (3M Ltd), such that a typical 6 × 6 mm square area in the centre of one face of the coupon was exposed to electrolyte. The Mg samples were completely immersed, exposed area uppermost, in an electrolyte bath containing aqueous sodium chloride electrolyte of varying concentration in the 0.01 to 1 mol dm^{-3} range at pH 6.5. Electrolyte pH was adjusted using appropriate additions of aqueous hydrochloric acid (HCl) or sodium hydroxide (NaOH). Time lapse photography was carried out using a computer-controlled Nikon D70S digital SLR camera fitted with an AF-micro close-up lens. Time-dependent free corrosion potential measurements were made using a Solartron 1280B Electrochemical workstation used in conjunction with a saturated calomel reference electrode.

Results and discussion

Influence of NaCl solution concentration

A series of experiments carried out using CP-Mg (280 ppm Fe impurity) specimens immersed in neutral, aqueous NaCl (aq) electrolyte at concentrations in the range 10^{-2} to 1 mol dm^{-3}, showed significant changes in localised corrosion morphology with decreasing [NaCl]. Localised corrosion at ≥ 0.1 mol dm^{-3} was characterised by the appearance of black spots on the exposed Mg surface within minutes of immersion, which rapidly developed into continuously expanding dark disc-like features, evolving significant streams of rising hydrogen bubbles. Eventually the dark regions impinged on each other and consumed the entirety of the original intact (uncorroded) surface. A detailed description of the localised behaviour of this form of Mg in concentrated NaCl (aq) aqueous solution is given in previous paper [2] and will not be discussed further in this work. Figure 1 shows typical corrosion morphologies observed at different [NaCl], where the influence of a 2 order of magnitude concentration change can be seen. At 0.1 mol dm^{-3} the propagation of a hemispherical dark feature is observed, closely resembling the appearance of the corroded surface at

Faraday Discussions Accepted Manuscript

 This journal is © The Royal Society of Chemistry 2012

higher [NaCl] (see Figs 1a and b). However, a further 10 fold concentration decrease produced a transformation in the nature of localised corrosion observed, as shown (at a slightly higher magnification) in Fig 1c. In this case, although several black spots marked the initiation of localised corrosion within 10 min of immersion, propagation was characterised by linear growth of dark areas, where continuously lengthening narrow (ca. filament-like features, typically between 0.01 and 0.03 mm wide, traversed the exposed surface. Visible evidence of hydrogen evolution was observed over a distance of up to 0.4 mm behind advancing filament front edges.

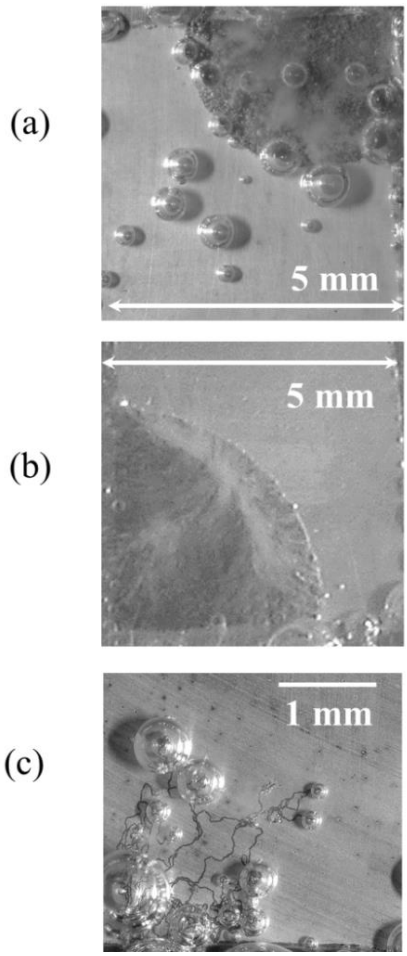

Figure 1: Photographic images taken in-situ of corroding CP-Mg surfaces held in (a) 1, (b) 0.1 and (c) 10^{-2} mol dm^{-3} NaCl (aq) at pH 6.5 after 40 min immersion.

From close up time-lapse photographic sequences recorded for the three immersion experiments summarised in Figure 1, propagation rates for both disc-form and filament-like corrosion could be estimated. In the case of the radial expansion of dark corroded regions observed in 1 and 0.1 mol dm^{-3} NaCl (aq), the rates were 1.3×10^{-3} and 1.0×10^{-3} mm/s respectively. An average rate of advance calculated for a selection of 10 individual corrosion filaments propagating in 10^{-2} mol dm^{-3} electrolyte was also 1.0×10^{-3} mm/s. The kinetics of corroded area growth in 1 mol dm^{-3} NaCl (aq), is discussed at length previously [2], demonstrating that the proportionality of corroded area (A) with the square of time, such that a plot of $(A)^{1/2}$ vs time was a good straight line with a slope of 1.9×10^{-3} mm s^{-1}. For linear FFC propagation observed in 0.01 mol dm^{-3} NaCl (aq), the area growth is proportional to time, typically producing a propagation rate of ca 3×10^{-3} mm^2 s^{-1}. As a result of the difference in corroded area growth rate laws, it is therefore difficult to make a direct comparison between disc-form corrosion and FFC in terms of the time-dependence of corroded area evolution. A full description of filiform corrosion (FFC) affecting CP-Mg under immersion in dilute NaCl electrolyte is given elsewhere [25] and will not be elaborated upon further here. The purpose of this work is therefore to explain how both types of corrosion morphology can be exhibited on the same type of Mg surface. To this end, the same set of immersion experiments were performed using in-situ, repetitive SVET scanning to determine time-dependent changes in local current density patterns under free corrosion conditions. Typical SVET-derived surface maps of current density along the axis of probe vibration (j_z) recorded at 40 min following immersion in 1.0, 0.1 and 10^{-2} mol dm^{-3} NaCl (aq) at pH 6.5 are shown in Figures 2a, b and c respectively.

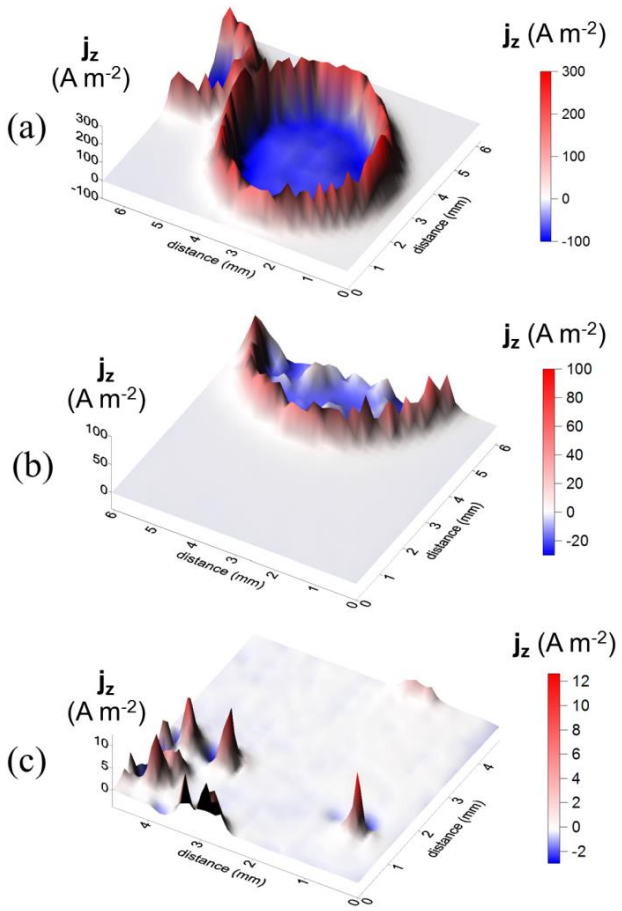

Figure 2: Surface plots showing the distribution of normal current density j_z above CP-Mg specimens freely corroding in (a) 1.0, (b) 0.1 and 10^{-2} mol dm^{-3} NaCl (aq) after 40 min immersion.

Faraday Discussions Accepted Manuscript

The SVET-derived map in Fig 2a for a CP-Mg specimen immersed in 1 mol dm^{-3} NaCl (aq) shows that the expanding disc-like dark areas comprise intense local anodes at their perimeter, with central regions becoming highly cathodically enhanced compared with the electrochemically inert, uncorroded surface. Previous work has demonstrated that disc-form corrosion propagation in concentrated NaCl (aq) is cathodically controlled, where anodic j_z values measured at corroded/intact region boundaries increase in proportion to the radius of local cathode regions within the expanding discs [2]. Although the experiment carried out in 0.1 mol dm^{-3} NaCl (aq) again shows similar localisation of anodic and cathodic activity, there is a distinct change in behaviour observed by in-situ SVET analysis. Initial scans, carried out within 30 min of immersion, again showed that local anodic activity was constrained to the perimeter of an expanding corrosion feature with intense cathodic activity located within its centre. However, at longer immersion times it became apparent that some local anodic activity had developed in a region of exposed blackened surface furthest from the anodic front. This is demonstrated in Fig 2b, where the corroded area on the upper right side of the j_z surface map shows net cathodic activity immediately behind the advancing anodic front, along with several anodic regions located a further distance to the rear. In addition, SVET mapping also revealed that the anodic intensity of the corrosion front did not vary with time as a progressively greater area of dark corroded surface was revealed. This is clearly demonstrated in the series of j_z versus distance profiles, taken along the radius of a propagating corrosion feature at different times following immersion in 0.1 mol dm^{-3} NaCl (aq), given in Figure 3. The magnitude of peak anodic j_z remains unchanged at ca +60 A m^{-2}, while plots ii – iv show clearly that the area of maximum cathodic current density of ca -30 A m^{-2} is located immediately behind the 0.5 mm wide anodic front. Fig 3 also shows that a region immediately in front of the initiation point, which is shown as a strong local cathode over the first 40 min of immersion, becomes transformed into a net local anode as the anodic front moves further forward (See Fig 3, curve v). This suggests that localised corrosion within this zone occurs independently of the apparent ongoing galvanic coupling of the anode at the disc perimeter with a ca. 2 mm wide cathodic zone immediately behind.

This observation of the onset of local anodic activity at protracted immersion times within a previously cathodic central region implies that decreased electrolyte conductivity is limiting the distances over which galvanic coupling can occur. As a consequence, the site of primary cathodic activity is thought to become constrained within an inner annular region concentric with the local anode maintained at the circumference of the expanding corrosion feature. This in turn differs from the case of the same Mg surface corroding in 1 mol dm^{-3} NaCl (aq), where the entirety of the interior of the expanding discs remain strong local cathodes over a similar period [2].

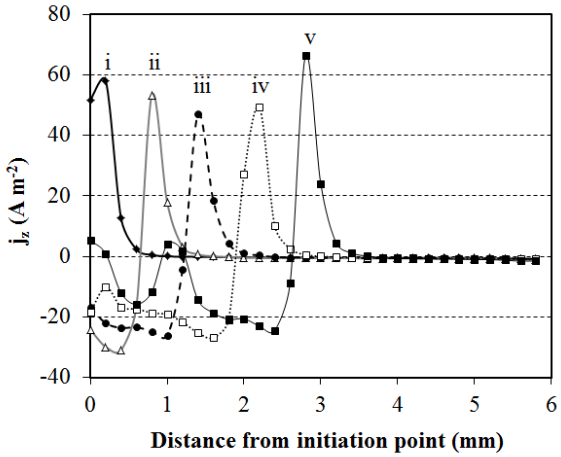

Figure 3: Normal current density j_z profiles taken along the radius of an expanding semi-circular corrosion feature on unpolarised CP-Mg immersed in 0.1 mol dm^{-3} NaCl (aq) at pH 6.5. Time key: (i) 6 min, (ii) 18 min and at 12 min intervals thereafter.

These local anode areas visualised at protracted immersion times appear to be stationary and do no propagate in the same manner to the unified front of anodic activity observed initially. A closer investigation of the original site of localised corrosion initiation for CP-Mg immersed in 0.1 M NaCl (aq), shows that the cathodic current density value at this location declines with time at a rate of 0.8 A m^{-2} min^{-1} ,from a starting value of ca -30 A m^{-2} , reaching zero after 40 min immersion. After this point a local anode develops at this location, which grows in intensity with time, reaching a relatively constant value of +20 A m^{-2} at longer immersion times. The rate of expansion of the principal semi-circular corrosion feature remains constant, despite the propagation of local anodes close to the original point of initiation. This implies that these features have no bearing on the anode-cathode coupling which produces the expanding anodic area at the intact-corroded area boundary. Again this is consistent with limited electrolyte throwing power, where ohmic constraints mean that regions which are separated by several mm from the main anodic region corrode independently of each other, where galvanic coupling of local anodes and cathodes can only occur over distances which are dictated by the bulk electrolyte conductivity. For this intermediate NaCl concentration, these distances appear to be in the order of 1 – 2 mm.

In the case of CP-Mg immersed in 10^{-2} mol dm^{-3} NaCl (aq), Fig 2c demonstrates that areas affected by FFC show significant localisation of corrosion, where the leading edges of the dark tracks are revealed as regions of intense focal anodic activity with measured j_z values of between +5 and +10 A m^{-2}. As the corrosion tracks propagate and anodic regions move away from their point of initiation, they leave behind regions of net cathodic activity with measured j_z values of up to -3 A m^{-2}. Again, the observed electro-catalytic activation of the corroded surface towards hydrogen evolution, according to reaction (1),

Faraday Discussions Accepted Manuscript

This journal is © The Royal Society of Chemistry 2012

is consistent with behaviour observed in higher concentration NaCl electrolyte.

$$2H_2O + 2e^- \rightarrow H_2 + 2OH^- \quad (1)$$

However, here the similarity ends, and the propagation of localised corrosion features involves linear growth of narrow dark tracks, rather than circular expansion of the black corroded surface. Although Fig 1c shows a "random-walk" type of propagation of filaments over the exposed Mg surface, where an individual track will change direction many times during the course of its advance, there are indications that the directionality is not stochastic. The anodic front edge of a filament cannot re-tread the same path back along its length because of a combination of elevated pH and impurity element enriched surface. There is also evidence in the literature that FFC propagation on Mg in 0.01 mol dm^{-3} NaCl (aq), albeit in the presence of a dilute chromate addition to the corrosive electrolyte, preferentially follows certain crystallographic features of the Mg grains and as a consequence the observed filament directionality is strongly influenced by changes in orientation at grain and twin boundaries [23].

The principal question to be asked is why the morphology should change so markedly at this lower concentration of corrosive electrolyte. Since it has been demonstrated that the corroded surface is capable of sustaining cathodic current densities which can be as high as -150 A m^{-2} in more concentrated aqueous NaCl solution [2], then the explanation must lie in the decreased conductivity of the electrolyte which limits the distance over which galvanic coupling can occur. Figure 4 shows a schematic representation of the proposed development of a circular corrosion feature after the initiation of localised corrosion.

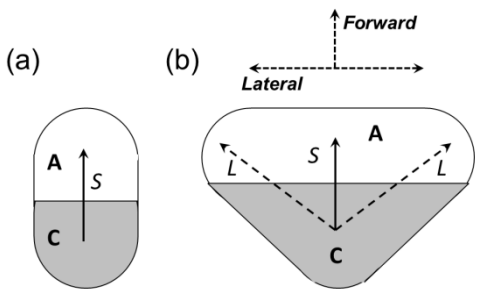

Figure 4: Schematic representation of the possible stages in the post-initiation evolution of localised corrosion on CP-Mg to give disc-form propagation. Local anode and cathode regions are labelled A and C respectively.

Previous work has shown that black spots, which mark the points of localised corrosion initiation, are intense, highly focal net anodes [2,4,25]. However, within a short space of time, the local anode moves away from its initiation point, leaving behind a cathodically activated region (see Fig 4a). Forward motion of the local anode is driven by electro-catalytic activation of the previously anodically-attacked surface with respect to reaction (1), while the local corrosion cell is maintained by ionic current flowing in the electrolyte via a short path indicated by arrow *S*. In order to propagate radially, the anode must be capable of moving both forward and laterally as indicated in Fig 4b. In highly conductive electrolyte, this is made possible by the ability of ionic current to flow along significantly longer paths, indicated by the arrows marked *L*. In turn, this allows the local anode to surround the cathodic site as shown in Fig 5a while simultaneously advancing away from the initiation site, leading to the formation of a circular corrosion feature comprising a cathode interior coupling with an anodic perimeter. However, in the case of dilute NaCl (aq) electrolyte shown in Fig 5b, where higher resistivity precludes the passage of ionic current over longer paths lengths *L*, only forward motion of the anode is possible, where the shortest possible ionic current path S completes the local corrosion cell coupling region C to region A. Additionally, in such a low throwing power electrolyte, only a relatively short length of the filament immediately behind the local cathode will be actively coupling with the local anode at its front edge. Therefore as a corrosion filament advances, cathodic j_z values measured along its length some distance behind the leading edge would be expected to progressively decrease with time. This was confirmed experimentally in previously published work [25].

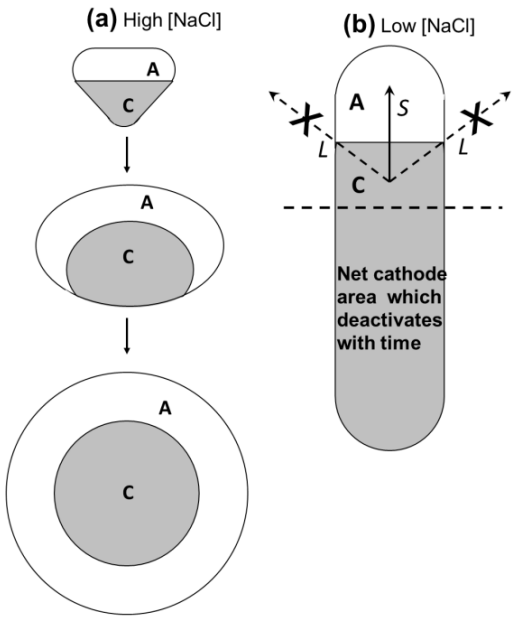

Figure 5: Schematic representation of the development of localised corrosion features on CP-Mg in (a) high and (b) low concentration NaCl electrolyte.

The effect of iron impurity level

In a separate series of experiments carried out using a test electrolyte comprising high throwing power NaCl (aq) at a fixed concentration of 1 mol dm^{-3}, the influence of iron impurity level on both the nature of the observed localised corrosion features and the corresponding current density

Faraday Discussions Accepted Manuscript

distributions were investigated. In such electrolyte there should be no ohmic constraints on localised corrosion propagation and galvanic coupling of local anodes and cathodes should be possible over significant distances. Four different types of iron containing Mg specimens were used for this study, spanning a composition range of 40 ppm up to 1.3×10^4 ppm. From preliminary immersion experiments, it became evident that Mg specimens containing ≥ 280 ppm Fe showed disc-form propagation of the dark corroded surface, while samples containing an iron impurity level below the commonly quoted high corrosion rate threshold of 170 ppm [34], (in this case two types of high purity Mg containing either 40 or 80 pm Fe) exhibited only filiform-like corrosion. Rapid radial expansion of dark corrosion discs for specimens containing either 1.3% w/w or 280 ppm Fe impurity led to the complete conversion of the original 36 mm^2 exposed area of uncorroded surface to a black, highly corroded surface within 90 min of immersion. The rate is marginally slower than that observed for CP-Mg (280 ppm Fe) specimens, where the entirety of the original surface was typically consumed within 60 min. In contrast, specimens comprising both 40 and 80 ppm Fe showed significantly slower rates of corrosion propagation as estimated by the area percentage of the total area affected by dark, corrosion tracks. Even after a maximum immersion period of 24h, only ca. 75% of the original intact working area had been affected by FFC activity for both types of low Fe impurity Mg specimen.

In-situ SVET analysis of the Mg-Fe (1.3%) specimen immersed in 1 mol dm^{-3} NaCl (aq), confirmed similar characteristics to the localised corrosion propagation of CP-Mg (280 ppm Fe) described previously and in detail elsewhere [2]. As demonstrated in Figure 6, a roughly circular corrosion feature, radially expanding at rate of 0.8×10^{-3} mm/s and characterised by a cathodic interior and anodic perimeter, is observed on the exposed surface. Peak j_z values of -150 A m^{-2} measured within the cathodically enhanced zone are roughly similar to those established on a corroding CP-Mg surface, despite the 50 fold decrease in iron impurity weight percentage. As observed previously for disc-like propagation, the expansion of the dark corroded region is again accompanied by a progressive increase in anodic j_z values measured at the intact-corroded surface boundary. However, despite the similarities in behaviour, some distinct differences were also observed, most notably the presence of a persistent permanent cathode seen in the lower quarter of Figs 6a and b, which was evident from the point of initial immersion. An unusual characteristic of local cathode, which evolved a permanent stream of hydrogen bubbles, was that the enhanced cathodic activity was not associated with a region of dark corroded surface and that this particular local cathode remained uncorroded at all times ≤ 60 min. Although post-corrosion chemical analysis was not carried out, it is proposed that this persistent cathode may have been associated with a region of surface heterogeneity comprising a large number of iron rich particles.

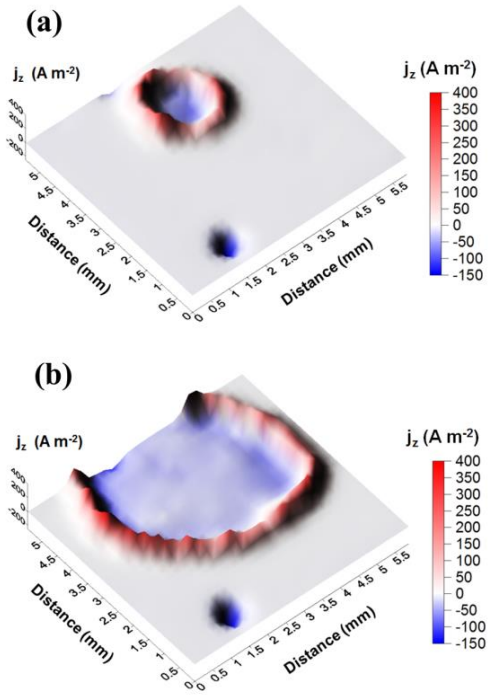

Figure 6: SVET-derived j_z surface maps showing the evolution of localised corrosion on a Mg-Fe (1.3% w/w) alloy after immersion in 1 mol dm^{-3} NaCl (aq) at pH 6.5 for (a) 15 and (b) 50 min.

For the highest purity Mg specimen (40 ppm), which was supplied as section of 10 mm diameter rod set in epoxy resin, the initiation and subsequent propagation of localised corrosion in 1 mol dm^{-3} NaCl (aq), visualised by in-situ SVET analysis, is summarised in Figure 7. The principal features are similar to those previously published [35], but under immersion in more dilute (0.1 mol dm^{-3}) electrolyte, where the point of breakdown after 30 min (Fig 7a) is revealed as an intense local anode, with the remainder of the uncorroded surface weakly cathodic (j_z up to -1 A m^{-2}). This local anode moves away its initial location and leaves behind a cathodically activated blackened track, showing significantly higher cathodic j_z values of up to -10 A m^{-2} than the intact surface. With time, more local anodes initiate and propagate in this vicinity of the exposed surface, eventually producing a network of dark filaments where the majority of the corroded surface is cathodically enhanced and anodic activity is limited to a few regions at the leading edge of these tracks (see Fig 7b and c).

The presence of a slightly higher Fe impurity level (80 ppm) did not greatly influence localised corrosion characteristics, as confirmed by Figure 8 which shows a j_z distribution map obtained after 12h immersion in 1 mol dm^{-3} NaCl (aq). A comparison with Fig 7c shows that both types of Mg specimen show a similar extent of corroded area over the same period of immersion. In addition, the magnitude of current density values measured for both anode and cathode areas on both type of

Faraday Discussions Accepted Manuscript

This journal is © The Royal Society of Chemistry 2012

surface were also similar, with j_z values of up to + 60 and -10 A m^{-2} established for local anode and cathode regions respectively.

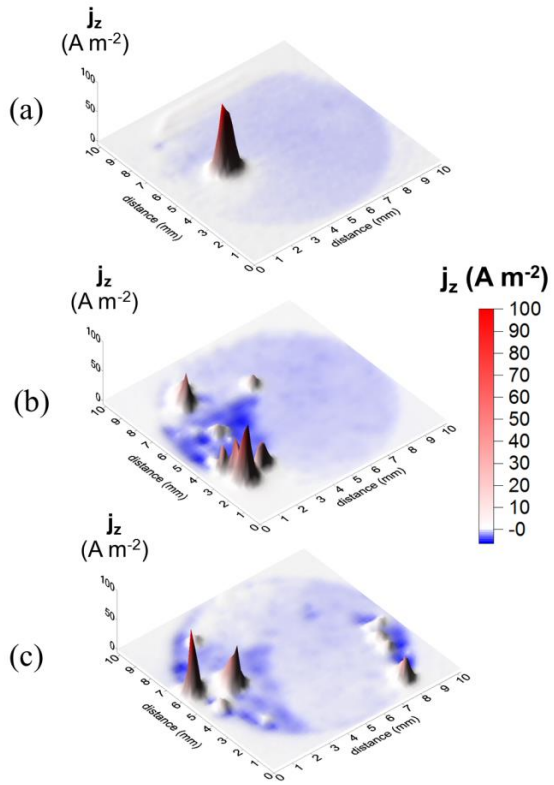

Figure 7: SVET-derived j_z surface maps showing the evolution of localised corrosion on a high purity (HP) Mg sample (40 ppm Fe) after immersion in 1 mol dm^{-3} NaCl (aq) at pH 6.5 for (a) 30 min, (b) 6h and (c) 12h.

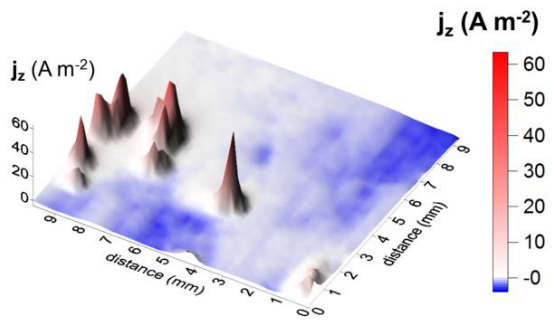

Figure 8: SVET-derived j_z surface map recorded after 12h immersion in 1 mol dm^{-3} NaCl (aq), showing localised corrosion patterns on an Mg sample containing 80 ppm Fe impurity

From these results it is evident that the magnitude of the cathodic current density which can be sustained on the dark, corroded surface is the main controlling factor in the propagation of localised corrosion on Mg surfaces in high throwing power corrosive electrolyte. High localised corrosion rates are observed on specimens having an iron impurity ≥ 280 ppm, which exhibit disc-form propagation, where current density values of up to -150 A m^{-2} can be maintained on the corroded surface. In contrast, localised corrosion propagation on high purity Mg, comprising Fe impurity levels well below the commonly-quoted 170 ppm threshold, take the form of linear filaments which advance at a significantly lower rate and can only sustain maximum cathodic current density values of -10 A m^{-2}. The large number of SVET-derived j_z surface maps of the types shown in Figures 6 - 8 can be effectively condensed by the estimation of time-dependent, area-averaged anodic current density (Ja_t) as described in previous publications [2,4,36,37]. This is achieved through the numerical area integration of j_z distributions using an approach outlined elsewhere [2,4,36,37] giving a description of the time-dependent evolution of localized corrosion currents in a compact manner. Figure 9 shows plots of Ja_t versus time, comparing the behaviour in 1 mol dm^{-3} NaCl of the various Mg specimen types comprising Fe impurity levels in the range 40 ppm up to 1.3% w/w. Ja_t is seen to increase rapidly with immersion time following breakdown for Mg specimens comprising ≥ 280 ppm Fig 9, plots 1 and ii, rising from a pre-breakdown value of 1 to ca 40 A m^{-2} after 60 min immersion. The subsequent drop to lower values approaching 10 A m^{-2} occurs because of a transition from localised to more general corrosion as the entirety of the working area is converted to a dark corroding surface.

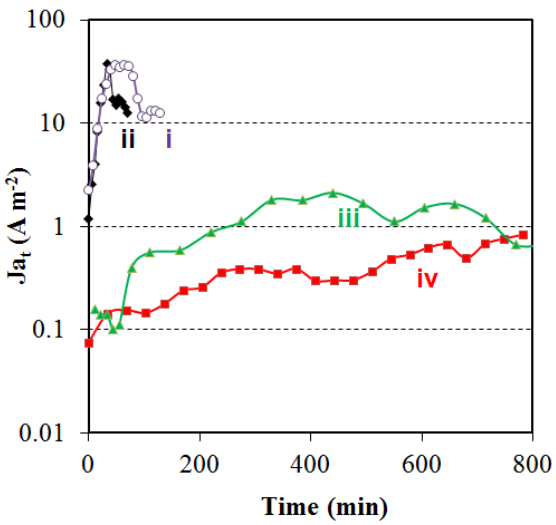

Figure 9: Area averaged integrated anodic current (Ja_t) plotted as a function of immersion time in 1 mol dm^{-3} NaCl (aq) for Mg specimens containing (i) 1.3 × 10^4, (ii) 280, (iii) 80 and (vi) 40 ppm Fe impurity.

The limitations of SVET in detecting corrosion events under situations where anode-cathode spacing becomes indistinct is discussed at length elsewhere [37]. However, in the case of both high purity Mg samples (≤ 80 ppm Fe), initial post-breakdown Ja_t values are an order of magnitude lower and rise significantly more slowly with time as FFC propagates over the exposed Mg

Faraday Discussions Accepted Manuscript

surfaces, reaching ca, 1 A m^{-2} after periods of immersion of greater than 6h. Figure 9 also confirms qualitative observations of greatly increased rates of corrosion at iron compositions of greater than 170 ppm, where time-dependent area-averaged current values rise at ca 1.0 A m^{-2} min^{-1} for curves i and ii. However, the corresponding increase observed for Mg specimens containing ≤ 80 ppm Fe impurity was roughly 5 × 10^{-3} A m^{-2} min^{-1}, representing a 500 fold reduction in localised corrosion rate increase.

It is not the main purpose of the work described here to establish why cathodic activation of the dark corroded regions occurs on Mg surfaces, or to offer an explanation about the controlling influence of iron impurity levels on the magnitude of cathodic current density values which can be sustained on these regions. Rather it is to point out that that the magnitude of latter dictates the morphology of localised corrosion propagation, which in turn controls the rate of corrosion. In a situation where ionic current can flow freely between local anode and cathode sites, cathodic current density values of -100 A m^{-2} or higher measured for low purity Mg supports circular propagation of the corroded surface, which in turn produces high rates of localised corrosion. In contrast, the low cathodic current density values of < -10 A m^{-2}, measured on the dark corroded surface produced on high purity Mg surfaces, are insufficient to sustain radial growth even in high conductivity electrolyte, and consequently only linear propagation of narrow dark corrosion tracks is observed, which in turn produces relatively low rates of localised corrosion. These observations on the influence of the magnitude of the iron impurity level tend to support theories which invoke iron-rich particle enrichment as the source of the observed cathodic activation of previously anodically-attacked Mg surface [2,5,14,16,38].

Influence of solution pH

Finally, it was demonstrated using CP-Mg (280 ppm Fe), that a transition from disc-form to linear corrosion propagation could also be produced in 1 mol dm^{-3} NaCl (aq) by increasing the bulk pH. Experiments carried out at bulk pH values of 10 and 12, showed very little change from neutral electrolyte, where disc-form propagation of dark regions was observed, with relatively little decrease in the rate of radial expansion of the localised circular corrosion features. In-situ SVET analysis again confirmed typical behaviour characterised by the presence of intense local anodes surrounding the discs, coupling with cathodically activated central interiors. At pH 12, typical j_z values measured for local cathodic regions were in the -50 to -80 A m^{-2} range, which is noticeably lower than values determined at pH ≤ 10. However, despite being lower at pH 12, the measured current density for cathodic hydrogen evolution remained sufficient to sustain disc-like corrosion growth, up to a point where the entire of the original "silvery" exposed surface became blackened.

A marked change in behaviour was observed when the bulk pH of the 1 mol dm^{-3} NaCl (aq) electrolyte was further raised to 13. Before immersion experiments were carried out, the pH 13 electrolyte was purged with synthetic air to remove any influence of dissolved carbon dioxide under conditions of high alkalinity. Despite the known increase in passivity of Mg produced at high pH [39], breakdown of the CP-Mg surface was observed within 6 min of immersion, characterised by the appearance of a small black spot on the exposed surface from which a stream of fine H_2 bubbles was evolved.

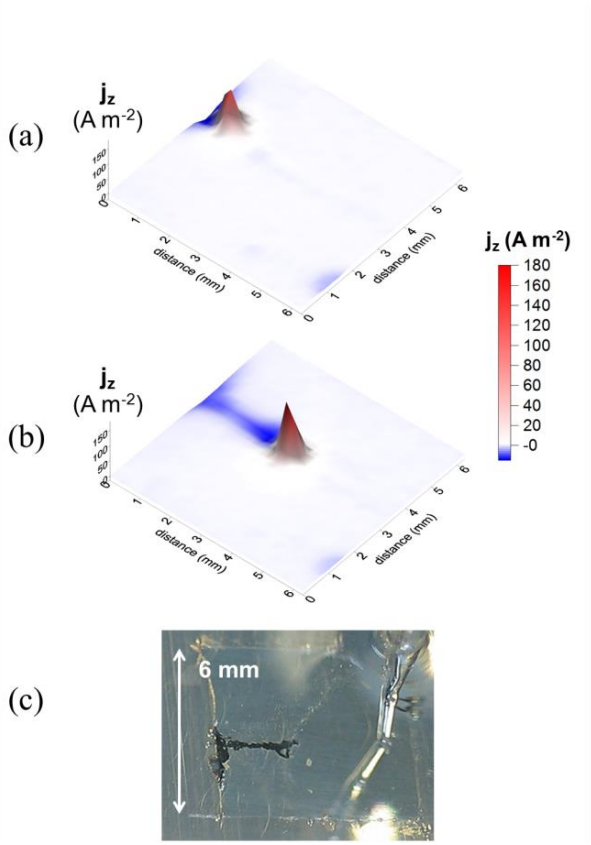

Figure 10: Surface plots showing the distribution of normal current density j_z above a CP-Mg specimen freely corroding in 1 mol dm^{-3} NaCl (aq) at pH 13, recorded after (a) 60 and (b) 90 min immersion. (c) shows a photographic image of the corroding surface taken in situ after 2h.

In-situ SVET analysis of the corroding surface showed that several regions of localised corrosion initiated over the first hour of immersion, but remained active only temporarily. However, after this period a dark region on the left edge of the exposed surface, as shown in Figure 10 developed into a propagating corrosion filament of roughly 0.5 mm width. As the SVET-derived j_z maps given in Figs 10a and 10b demonstrate, the propagating track comprises an intense local anode at its front edge, with the reminder of the track revealed as cathodically activated with respect to the intact (uncorroded) surface. As the track lengthens, there is no evident change in the anodic current density measured at its leading edge. This is confirmed in Figure 11, which shows profiles of current density versus distance taken along the length of the propagating

Faraday Discussions Accepted Manuscript

This journal is © The Royal Society of Chemistry 2012

corrosion filament at different immersion times. Peak anodic j_z is reasonably constant at ca +180 A m^{-2}, while cathodic values of up to -20 A m^{-2} are typically highest in a region immediately behind the advancing anode (see Fig 11, curve iii). A velocity of 10^{-3} mm/s was estimated for the propagating track shown in Fig 10, which is entirely similar to values determined for localised corrosion features observed on CP-Mg immersed at pH 6.5 in NaCl (aq) electrolyte at concentrations of ≤ 0.1 mol dm^{-3}. A final question in this case arises about why radial propagation occurs for CP-Mg in 1 mol dm^{-3} NaCl solution at near neutral values up to pH 12, but transforms to filiform-like propagation at pH 13.

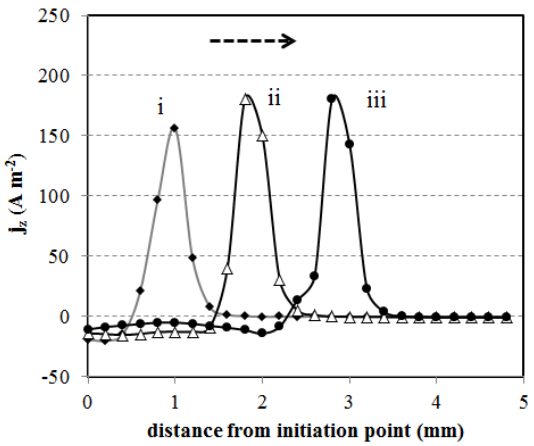

Figure 11: Normal current density j_z profiles taken along the radius of a propagating corrosion track on unpolarised CP-Mg immersed in 1 mol dm^{-3} NaCl (aq) at pH 13. Time key: (i) 60 min, (ii) 72 min and (iii) 84 min. The arrow indicates the direction of propagation.

If the observed change in morphology is due to the greater passivity of the uncorroded Mg surface at high pH, then this would be expected to affect the initiation of localised corrosion, probably by significantly lengthening the time delay to breakdown under unpolarised conditions. However, the fact breakdown is observed within minutes of immersion in the absence of external polarisation suggests that this facet of localised corrosion is relatively unaffected by elevated pH and rather it is the propagation phase which is predominately influenced. In this respect, this finding is consistent with observations of the localised corrosion behaviour of Mg alloy AZ31 over a range of bulk pH values in concentrated aqueous NaCl electrolyte [3]. Therefore the transition to linear propagation again seems to derive from the relatively low (up to -20 A m^{-2}) cathodic current that is generated on the corroded, darkened surface, which in turn is below the empirically derived threshold which seems to be required to sustain radial growth over significant distances. A progressive decrease in mean cathodic current density values determined at pH values of 10, 12 and 13 of -140, -80 and -15 A m^{-2} respectively is consistent with pH dependence of the electrochemical potential of the hydrogen evolution reaction (1) with pH given below [39].

$$E_{H2} = E° - 0.0591pH \quad (2)$$

The open circuit potential of CP-Mg was shown to be unaffected by an increase in electrolyte pH to 13, where E_{corr} was ca 40 mV more positive than the value of -1.4 V vs. SHE measured in neutral 1 mol dm^{-3} NaCl (aq). If it assumed that local cathode sites are polarised to -1.36 V vs. SHE then a progressive increase in pH will lead to decrease in the magnitude of cathodic polarisation for H_2 evolution From equation (2) that cathodic it can be calculated that the overpotential for cathodic HER at pH 13 is reduced by 0.42 V compared with neutral conditions. This appears to be sufficient to markedly de-activate cathodic hydrogen evolution on iron-impurity enriched, corroded regions.

Conclusions

The localised corrosion of unpolarised Mg specimens, comprising varying iron impurity levels, shows propagating features which appear to be governed by the magnitude of the cathodic current density which is maintained on the dark, anodically-attacked surface. In-situ SVET was used to demonstrate that circular expansion of dark corroded regions in concentrated NaCl (aq) solution occurred under circumstances where cathodic current densities of -100 A m^{-2} or higher were measured within a central portion of a disc-like feature comprising a strong local circumferential anode. Such values were established on Mg specimens which contain iron impurity levels of ≥ 280 ppm and led to high rates of localised corrosion as quantified by numerical area integration of SVET-derived current density maps. In contrast, cathodic current density values of -10 A m^{-2} or lower were measured on the dark corroded surface produced on high purity Mg specimens immersed in the same corrosive electrolyte. These relatively low currents were shown to be insufficient to generate radial expansion of the corroded surface, and consequently only linear propagation to give filament-like features was observed. Unsurprisingly, rates of localised corrosion quantified by the magnitude of time-dependent, SVET-derived integrated anodic currents were over 2 orders of magnitude lower on Mg specimens containing ≤ 80 ppm Fe impurity levels.

In separate experiments using commercial purity Mg containing 280 ppm Fe impurity, the influence of NaCl electrolyte concentration on localised corrosion propagation was investigated. At concentrations ≥ 0.1 mol dm^{-3}, disc-form corrosion is observed, where the expansion of the local anode at the perimeter is sustained by cathode current density values of greater than -30 A m^{-2} within the interior of the disc. However, when the concentration is further decreased by an order of magnitude, only filiform corrosion (FFC) is observed, indicating ohmic constraints which produce linear rather than radial localised corrosion propagation. A similar effect is produced in 1 mol dm^{-3} NaCl (aq) by increasing the bulk pH to 13. In this case, where the high throwing power electrolyte

Faraday Discussions Accepted Manuscript

should not constrain ionic current paths, the transition from radial to linear propagation resulted from the relatively low cathodic current density of ca -15 A m^{-2} which was measured over the corroded surface.

Acknowledgements

M. A. Gibson (CSIRO/CAST-CRC) is gratefully acknowledged for assistance in preparing the Mg-Fe alloy. Prof A. Atrens (University of Queensland) is thanked for the gift of high purity Mg containing an 80 ppm iron impurity level.

Notes and references

[a] Materials Research Centre, College of Engineering, Swansea University, Singleton Park, Swansea, UK, SA2 8PP.

[b] Department of Materials Engineering, Monash University, Clayton, Victoria VIC 3800, Australia

1 M. E. Straumanis and B. K. Bhatia, J. Electrochem. Soc, 1963, **110**, 357

2 G. Williams and H.N. McMurray, *J. Electrochem. Soc*., 2008, **155,** B340**.**

3 G. Williams, H. ap Llwyd Dafydd and R. Grace, *Electrochim. Acta*, 2013, **109**, 489.

4 G. Williams, N. Birbilis and H.N. McMurray, Electrochem. Commun., 2013, **36**, 1.

5 M. Curioni, *Electrochim. Acta*, 2014, **120**, 284.

6 G.L. Makar and J. Kruger, *Int. Mater. Rev*. 1993, **38**, 138.

7 G. Song and A. Atrens, *Adv. Eng. Mater*. 1999, **1**, 11.

8 G. Song and A. Atrens, *Adv. Eng. Mater*. 2003, **5**, 837.

9 E. Ghali, W. Dietzel and K.U. Kainer, *J. Mater. Eng. Perf*., 2004, **13**, 7.

10 G. Song, *Adv. Eng. Mater*., 2005, **7**, 563.

11 R. Zeng, J. Zhang, W. Huang, W. Dietzel, K.U. Kainer, C. Blawert and K.E. Wei, *Trans. Nonferrous Met. Soc. Chi.*, 2006, **16**, s763.

12 E. Ghali, Corrosion resistance of Aluminium and Magnesium alloys, John Wiley and Sons, New Jersey USA, (2010).

13 N.T. Kirkland, N. Birbilis and M.P. Staiger, *Acta Biomaterialia*, 2012, 8, 925.

14 J. Światowska, P. Volovitch and K. Ogle, *Corros. Sci*., 2010, **52,** 2372.

15 N. Kirkland, G. Williams, and N. Birbilis, *Corros. Sci*., 2012, **65**, 5.

16 N. Birbilis, A.D. King, S. Thomas, G.S. Frankel, J.R. Scully, *Electrochim. Acta*, 2014, **132**, 277.

17 G.S. Frankel, A. Samaniego and N. Birbilis, *Corros. Sci*, 2013, **70**, 104.

18 J.W. Turrentine, *J. Phys. Chem*, 1908, **12,** 448.

19 R.L. Petty, A.W. Davidson and J. Kleinberg, *J. Am. Chem. Soc*., 1954 **76**, 363.

20 G. Song, A. Atrens, D. St John, J. Nairn, Y. Li, *Corros. Sci*., 1997, **39**, 855.

21 A. Atrens and W. Dietzel, *Adv. Eng. Mater*., 2007, **9,** 292.

22 T.R. Thomaz, C.R. Weber, T. Pelegrini, L.F.P. Dick and G. Knornschild, *Corros. Sci.* 2010, **52**, 2235.

23 Z.M. Shi, J.X. Jia and A. Atrens, *Corros. Sci*. 2012, **60,** 296.

24 P. Schmutz, V. Guillaumin, R.S. Lillard, J.A. Lillard and G.S. Frankel, *J. Electrochem. Soc*., 2003, **150**, B99.

25 G. Williams and R. Grace, *Electrochim. Acta*, 2011, **56**, 1894.

26 O. Lunder, J.E. Lein, S.M. Hesjevik., T.K. Aune, K. Nisancioglu, *Werkst. Korros.*, 1994, **45**, 331.

27 C. Liu, Y. Xin, G. Tang, P. K. Chu, *Mater. Sci. Eng: A*, 2007, **456**, 350.

28 S. Izumi, M. Yamasaki and Y. Kawamura, *Corros. Sci*., 2009, **51**, 395.

29 Y.W. Song, D.Y. Shan, R.S. Chen and E.H. Han, *Corros. Sci*., 2009, **51**, 1087.

30 J. R. Kish, G. Williams, J. R. McDermid, J. M. Thuss and C. F. Glover, *J. Electrochem. Soc*. 2014, **161**, C405.

31 G. Williams, K. Gusieva and N. Birbilis, *Corrosion*, 2012, **68**, 489.

32 S. Simanjuntak, M.K. Cavanaugh, D.S. Gandel, M.A. Easton, M.A. Gibson and N. Birbilis, *Corrosion*, 2014, DOI: 10.5006/1467

33 G. Williams and H.N. McMurray, *Corrosion*, 2006, **62**, 231.

34 R.E. McNulty and J.D. Hanawalt, *Trans. Electrochem. Soc.*, 1942, **81**, 423.

35 K.D. Ralston, G. Williams and N. Birbilis, *Corrosion*, 2012, **68**, 507.

36 G. Williams, H.N. McMurray and R. Grace, *Electrochim. Acta*, 2010, **55,** 7824.

37 G. Williams, A.J. Coleman and H.N. McMurray, *Electrochim. Acta*, 2010, **55**, 5947.

38 M. Taheri, J.R. Kish, N. Birbilis, M. Danaie, E.A. McNally, J.R. McDermid, *Electrochim. Acta*, 2014, **116**, 396.

39 M. Pourbaix (Ed.), Atlas of Electrochemical Equilibria in Aqueous Solutions, Pergamon Press, London, 1966.

Faraday Discussions Accepted Manuscript

 This journal is © The Royal Society of Chemistry 2012